Microscopic approach for the site distribution and thermodynamic properties of a single-component polymer subjected to an external field

Shiqi Zhou and Xiaoqi Zhang
Research Institute of Modern Statistical Mechanics, Zhuzhou Institute of Technology, Wenhua Road, Zhuzhou City 412008, People's Republic of China

(Received 28 November 2000; published 25 June 2001)

A microscopic statistical mechanics approach is proposed for a nonuniform single-component freely jointed tangential hard-sphere polymer in the framework of density-functional theory. The present approach avoids the use of single-chain simulation in the theory by treating bonding interaction on the basis of the properties of the Dirac δ function. The present excess free energy includes all terms of functional perturbative expansion around the uniform bulk fluid in the form of the Verlet-modified bridge function. The second-order direct correlation function of a uniform polymer melt as the input parameter is obtained by solving numerically the polymer–reference-interaction-site-model integral equation with the Percus-Yevick closure. Predictions of the present approach for such microscopic structural and thermodynamics properties as the site density distribution, the partition coefficient, and the adsorption isotherm near a hard wall or between two hard walls are compared with computer-simulation results and with those of previous theories. The comparison indicates that the present approach is more accurate than the previous integral equation theory and the most accurate Monte Carlo density-functional theories. The predicted oscillations of the medium-induced force between two hard walls immersed in polymer melts are consistent with the experimental results available in the literature. The relation of the present approach with self-consistent-field theory, as well as the differences between the two, are discussed.

DOI: 10.1103/PhysRevE.64.011112 PACS number(s): 05.20.−y

I. INTRODUCTION

It is well known that an oscillatory local-density distribution is generated in a hard sphere fluid adjacent to a solid surface. The formation of the oscillatory local-density distribution is due to the so-called packing effect, which modifies the local environment of near-surface particles by reducing the number of short-ranged interactions these particles have with other particles. However, when hard spheres are connected to hard sphere chains, another feature comes into play that is imposed by the connectivity of the monomers in the chain. This feature is called the entropic penalty effect because the highly repulsive surface reduces the number of conformations of the chains near the surface. The competition between these two effects leads to various polymer interfacial behaviors, such as a modified oscillatory local-density distribution [1] compared with a hard sphere fluid near a surface, surface depletion [2], etc. A large number of technical applications of polymer melts exploits their interfacial or surface properties to control surface-fluid interactions and surface-surface interactions [3]. However, the behaviors of polymer melts near a surface have been studied experimentally much less because most high molecular weight polymers have high viscosities, thus making equilibrium measurements highly difficult. This situation makes theoretical methods highly necessary.

There are several theoretical methods for the description of a polymer melt near a surface. A scaling methodology was formulated by DeGennes [4] which is valid for sufficiently long polymers and provides general properties without a detailed description of monomers. The Flory mean-field lattice model for uniform polymers was extended to the nonuniform case by Scheutjens and Fleers [5]. This theory is suitable for all chain lengths and can be easily adapted to various boundary conditions. However, it cannot provide detailed structural information due to the noncontinuous lattice model approximation employed. The theory of Scheutjens and Fleers was extended to continuous space by Bjorling and Linse [6]. Liquid state methods, such as the integral equation theory for uniform fluids, could also be extended to the nonuniform case. For example, Yethiraj and Hall [7] used the polymer-RISM (reference interaction site model) theory of Curro and Schweizer [8] coupled with the growing adsorbent model of Henderson *et al.* [9] and its extension to slitlike pores by Zhou and Stell [10] to develop an integral equation theory for chain molecules in slitlike pores. The density-functional theory constitutes a fourth class of approaches, which are the most popular and suitable theories for nonuniform fluids. In this category, an early version has made use of intuitive, phenomenological expressions for the thermodynamics potential [11] that, when minimized, provided the equilibrium properties of the studied system. However, these phenomenological approaches often entailed adding to the bulk free-energy functional ad hoc term contributions that allowed the adsorption or desorption of monomers, thus this version is not completely satisfactory from a theoretical point of view. Lately, Chandler *et al.* [12,13] have extended the density-functional theory of nonuniform atomic fluids to nonuniform polyatomic species, McMullen and Freed [14] have derived a density-functional formulation from basic statistical mechanics relations, and Woodward [15] has derived the so-called generalized van der Waals density-functional theory to the nonuniform polymer case. A density-functional theory for uniform and nonuniform polymers is also developed by Kierlik and Rosinberg [16–18], which constitutes an extension of Wertheim's first-order thermodynamic perturbation theory [19–22] of polymerization in the limit of complete association. In addition, two Monte Carlo density-functional

theories are proposed by Yethiraj and Woodward [23] and by Yethiraj [24]. Finally, computer simulations [25,26] provided the most detailed and exact description of nonuniform polymer systems. Among the above methods, the density-functional theories [15,18,23,24] are more accurate than the integral equation theory [7], which in turn is somewhat more accurate than the self-consistent-field theory of Bjorling and Linse [6]. The DFT's and integral equation theory (IET) can provide detailed structural descriptions that are beyond the scope of scaling theory and self-consistent-field theory by Scheutjens and Fleers. Among the DFT's, the Monte Carlo DFT's combine the undesirable features of both simulation and theory. While approximate, they still require computer simulations. However, the DFT's of Refs. [16–18] are even more demanding computationally than the Monte Carlo DFT's, but are rigorous from the theoretical point of view. The DFT of Ref. [15] is modest computationally when compared to those of Refs. [23], [24], [16–18], but still requires vectorized calculations and furthermore contains an adjustable parameter. The DFT's of Refs. [12] and [13] also require single-chain simulations when carried out computationally [27], and the DFT formulations of Ref. [14] are not yet carried out numerically. The computer simulations have the advantage of being conceptually simple and numerically exact, but the disadvantage of being demanding computationally, especially for polymers near a surface because of the enhanced local density and the associated reduction in chain mobility. At present, they only serve as standard tools for verifying the theory when experimental data are not available.

The present paper is based on the idea of the universality of the free-energy density functional, the aim being to construct a numerically modest (without resort to the single-chain simulation) and quantitatively more accurate DFT. Section II contains the formulation of the present DFT and a discussion regarding its numerical solution. In Sec. III, the predictions of the present DFT are compared with computer-simulation results and those of the previous DFT's and integral equation theory. Finally, Sec. IV contains some concluding remarks. A detailed derivation of Eq. (18) is included in the Appendix.

II. DENSITY FUNCTIONAL THEORY

A. Formulation of the new DFT formalism

We consider a polymer model consisting of N_p freely jointed tangential hard spheres of diameter σ, free of any inherent angular bonding stiffness apart from monomer repulsion, and with the bonding potential $v_p(r)$ between successive monomers in the chain dependent only on the distance between the centers of the successive monomers. The total bonding potential $V_p(\mathbf{R})$ corresponding to an arbitrary configuration of a polymer chain $\mathbf{R}=(\mathbf{r}_1,\mathbf{r}_2,\ldots,\mathbf{r}_n)$ is the sum of all the nearest-neighbor bonding potentials, that is,

$$V_p(\mathbf{R})=\sum_{i=1}^{N_p-1} v_p(|\mathbf{r}_{i+1}-\mathbf{r}_i|). \tag{1}$$

We consider the tangential hard spheres chain, so there is a fixed bonding length σ. The covalent bonding potential is represented by

$$v_p(r)=k(r-\sigma)^2, \tag{2}$$

where k is the force constant tending to infinity.

In the density-functional theory, all equilibrium properties are obtained by requiring that the system grand potential $\Omega[\rho_p(\mathbf{R})]$ be stationary with respect to changes in the polymer molecule local-density distribution $\rho_p(\mathbf{R})$, that is [28],

$$\frac{\delta\Omega[\rho_p(\mathbf{R})]}{\delta\rho_p(\mathbf{R})}=0. \tag{3}$$

The grand potential functional $\Omega[\rho_p(\mathbf{R})]$ is related to the system Helmholtz free-energy functional $F[\rho_p(\mathbf{R})]$ by the Legendre transform

$$\Omega[\rho_p(\mathbf{R})]=F[\rho_p(\mathbf{R})]+\int[\Phi_{\text{ext}}(\mathbf{R})-\mu]\rho_p(\mathbf{R})d\mathbf{R}, \tag{4}$$

where μ is the chemical potential of a polymer molecule and $\Phi_{\text{ext}}(\mathbf{R})$ is the external potential. As in the procedure employed for simple atomic fluids, $F[\rho_p(\mathbf{R})]$ can be expressed by the sum of an ideal part $F_{\text{id}}[\rho_p(\mathbf{R})]$ and an excess part $F_{\text{ex}}[\rho_p(\mathbf{R})]$,

$$F[\rho_p(\mathbf{R})]=F_{\text{id}}[\rho_p(\mathbf{R})]+F_{\text{ex}}[\rho_p(\mathbf{R})]. \tag{5}$$

We express the above functional in terms of the polymer molecule local-density distribution $\rho_p(\mathbf{R})$, not the site density, consequently the ideal free-energy expression of simple atomic fluids can be extended to the case of polymers,

$$F_{\text{id}}[\rho_p(\mathbf{R})]=kT\int\rho_p(\mathbf{R})[In\rho_p(\mathbf{R})-1]d\mathbf{R}+\int\rho_p(\mathbf{R})V_p(\mathbf{R})d\mathbf{R}. \tag{6}$$

Combining Eqs. (3)–(6) leads to

$$\rho_p(\mathbf{R})=\exp\left\{-\beta\Phi_{\text{ext}}(\mathbf{R})-\beta V_p(\mathbf{R})+\beta\mu-\beta\frac{\delta F_{\text{ex}}[\rho_p(\mathbf{R})]}{\delta\rho_p(\mathbf{R})}\right\}, \tag{7}$$

where $\beta=1/kT$ is the reciprocal temperature, k is the Boltzmann constant, and T is the absolute temperature. In the present paper, we consider only the polymer melts whose segments are identical, therefore the average site density $\rho(\mathbf{r})$ is related to the polymer molecule local-density distribution $\rho_p(\mathbf{R})$ via

$$\rho(\mathbf{r})=\int\sum_{i=1}^{N_p}\delta(\mathbf{r}-\mathbf{r}_i)\rho_p(\mathbf{R})d\mathbf{R}. \tag{8}$$

Consequently,

$$\frac{\delta\rho(\mathbf{r}_i)}{\delta\rho_p(\mathbf{R})}=\frac{\delta\int\sum_{i=1}^{N_p}\delta(\mathbf{r}_i-\mathbf{r}_i')\rho_p(\mathbf{R}')d\mathbf{R}'}{\delta\rho_p(\mathbf{R})}$$
$$=\int\sum_{i=1}^{N_p}\delta(\mathbf{r}_i-\mathbf{r}_i')\,\delta(\mathbf{R}-\mathbf{R}')dR'$$
$$=\sum_{i=1}^{N_p}\int\delta(\mathbf{r}_i-\mathbf{r}_i')\,\delta(\mathbf{R}-\mathbf{R}')d\mathbf{R}'=N_p\,, \qquad (9)$$

therefore

$$\frac{\delta F_{\mathrm{ex}}[\rho_p(\mathbf{R})]}{\delta\rho_p(\mathbf{R})}=\sum_{i=1}^{N_p}\frac{\delta F_{\mathrm{ex}}[\rho_p(\mathbf{R})]}{\delta\rho(\mathbf{r}_i)}. \qquad (10)$$

Because the segments of the polymer chains are identical, the external potential that acts on a polymer molecule is given by

$$\Phi_{\mathrm{ext}}(\mathbf{R})=\sum_{i=1}^{N_p}\varphi_{\mathrm{ext}}(\mathbf{r}_i), \qquad (11)$$

where $\varphi_{\mathrm{ext}}(\mathbf{r})$ is the external potential felt by a segment of a polymer chain whose center is situated at $\mathbf{r}$.

Substituting Eqs. (10) and (11) into Eq. (7) leads to

$$\rho_p(\mathbf{R})=\exp\Bigg\{-\beta\sum_{i=1}^{N_p}\varphi_{\mathrm{ext}}(\mathbf{r}_i)-\beta V_p(\mathbf{R})+\beta\mu-\beta\sum_{i=1}^{N_p}\frac{\delta F_{\mathrm{ex}}[\rho_p(\mathbf{R})]}{\delta\rho(\mathbf{r}_i)}\Bigg\}. \qquad (12)$$

In the absence of an external potential (a uniform system), Eq. (12) acquires the following form:

$$\rho_p^b=\exp\Bigg\{\beta\mu-\beta\sum_{i=1}^{N_p}\left(\frac{\delta F_{\mathrm{ex}}[\rho_\rho(\mathbf{R})]}{\delta\rho(\mathbf{r}_i)}\right)_{\rho(r)\to\rho_b}\Bigg\}, \qquad (13)$$

where ρ_p^b is the bulk polymer molecule density related to the bulk segment density ρ^b by

$$\rho_p^b=\rho^b/N_p\,. \qquad (14)$$

One may notice that the term $\beta V_p(\mathbf{R})$ disappears from Eq. (13) due to the fact that use of the notation ρ_p^b means that $|\mathbf{r}_{i+1}-\mathbf{r}_i|=\sigma$ for $i=1,2,N_p-1$, thus $V_p(\mathbf{R})=\sum_{i=1}^{N_p-1}\nu_p(|\mathbf{r}_{i+1}-\mathbf{r}_i|)=\sum_{i=1}^{N_p-1}k(|\mathbf{r}_{i+1}-\mathbf{r}_i|-\sigma)^2=0$. But it exists in Eq. (12) because at this time it is not necessarily that $|\mathbf{r}_{i+1}-\mathbf{r}_i|=\sigma$ for $i=1,2,N_p-1$, however the condition $|\mathbf{r}_{i+1}-\mathbf{r}_i|=\sigma$ for $i=1,2,N_p-1$ will be realized in Eq. (28).

Equations (12) and (13) lead to

$$\rho_p(\mathbf{R})=\rho_p^b\exp\Bigg\{-\beta\sum_{i=1}^{N_p}\varphi_{\mathrm{ext}}(\mathbf{r}_i)-\beta V_p(\mathbf{R})-\beta\sum_{i=1}^{N_p}\frac{\delta F_{\mathrm{ex}}[\rho_p(\mathbf{R})]}{\delta\rho(\mathbf{r}_i)}+\beta\sum_{i=1}^{N_p}\left(\frac{\delta F_{\mathrm{ex}}[\rho_p(\mathbf{R})]}{\delta\rho(\mathbf{r}_i)}\right)_{\rho(\mathbf{r})\to\rho^b}\Bigg\}. \qquad (15)$$

The exact expression of $F_{\mathrm{ex}}[\rho_p(\mathbf{R})]$ is not known, but for $N_p=1$,

$$-\beta\frac{\delta F_{\mathrm{ex}}[\rho_p(\mathbf{R})]}{\delta\rho(\mathbf{r})}=c^{(1)}(\mathbf{r};[\rho(\mathbf{r})]) \qquad (16)$$

and

$$-\beta\left(\frac{\delta F_{\mathrm{ex}}[\rho_p(\mathbf{R})]}{\delta\rho(\mathbf{r})}\right)_{\rho(\mathbf{r})\to\rho^b}=C_0^{(1)}(\rho^b), \qquad (17)$$

where $C^{(1)}(\mathbf{r};[\rho(\mathbf{r})])$ and $C_0^{(1)}(\rho^b)$ are the first-order direct correlation functions for a nonuniform and a uniform atomic fluid, respectively. On the basis of the universality of the free-energy density functional, we derive in the Appendix [29] the following relationship between $C^{(1)}(\mathbf{r};[\rho(\mathbf{r})])$ and $C_0^{(1)}(\rho^b)$:

$$C^{(1)}(\mathbf{r};[\rho(\mathbf{r})])=C_0^{(1)}(\rho^b)+\int d\mathbf{r}_1[\rho(\mathbf{r}_1)-\rho^b]C_0^{(2)}\times(|\mathbf{r}-\mathbf{r}_1|;\rho^b)+B\Bigg[\int d\mathbf{r}_1[\rho(\mathbf{r}_1)-\rho^b]C_0^{(2)}\times(|\mathbf{r}-\mathbf{r}_1|;\rho^b)\Bigg], \qquad (18)$$

where $C_0^{(2)}(|\mathbf{r}-\mathbf{r}_1|;\rho^b)$ is the second-order direct correlation function of a uniform atomic fluid, $B(\gamma)$ is the bridge function of a uniform atomic fluid,

$$\gamma=h-C_0^{(2)} \qquad (19)$$

is the indirect correlation function, and h is the total correlation function, which is related to the radial distribution function g via

$$h=g-1. \qquad (20)$$

Regarding the bridge function, the Percus-Yevick (PY) [30] bridge function has the form

$$B[\gamma(\mathbf{r})]=In[1+\gamma(\mathbf{r})]-\gamma(\mathbf{r}) \qquad (21)$$

and the Verlet-modified (VM) [31] bridge function the form

$$B[\gamma(\mathbf{r})]=-\gamma(\mathbf{r})^2/2[1+4/5\gamma(\mathbf{r})]. \qquad (22)$$

In Ref. [29], we combined Eq. (18) with the density profile equation,

$$\rho(\mathbf{r})=\rho^b \exp\{-\beta\varphi_{\rm ext}(\mathbf{r})+C^{(1)}(\mathbf{r};[\rho])-C_0^{(1)}(\rho^b)\}, \tag{23}$$

to predict the density distribution of a nonuniform hard sphere fluid for several cases. We found that the most accurate predictions came from the use of the PY analytical expression for $C_0^{(2)}(|\mathbf{r}-\mathbf{r}_1|;\rho^b)$ and the VM bridge function.

The relationship Eq. (18) is now applied to polymer melts with $C_0^{(2)}(|\mathbf{r}-\mathbf{r}_1|;\rho^b)$ determined by solving the polymer reference interaction site model (PRISM) integral equation for the site-average correlation function [8,32],

$$h(r)=\int d\mathbf{r}'\int d\mathbf{r}''w(|\mathbf{r}-\mathbf{r}'|)C_0^{(2)} \times(|r'-\mathbf{r}''|;\rho^b)[w(r'')+\rho^b h(r'')] \tag{24}$$

coupled with the closure equation

$$g(r)=\exp[-1/kT\phi(r)+h(r)-C_0^{(2)}(r;\rho^b)+B(r)]. \tag{25}$$

The PY bridge function Eq. (21) will be used, because the PRISM theory based on the PY bridge function [33] provided good predictions for uniform polymer systems at both high and low densities, while the hypernetted-chain (HNC) and Martynov-Sarkisov (MS) bridge functions exhibited unphysical features and ultimately failed to converge at low densities and/or long chains.

The reasons for the above extension are as follows (i) Equation (18) can be recovered from its extended form (the PRISM integral equation reduces to the OZ equation when $N_p=1$). (ii) Equation (18) is the functional expansion of $C^{(1)}(\mathbf{r};[\rho(\mathbf{r})])$ about $C_0^{(1)}(\rho^b)$, the second term of the right-hand side of Eq. (18) is the main expansion term, and the third term only includes the residue. The second-order direct correlation functions $C_0^{(2)}(|\mathbf{r}-\mathbf{r}_1|;\rho^b)$ for uniform polymers and uniform atomic fluids are all second-order functional derivatives of the excess Helmholtz free energy with respective to the density distribution $\rho(\mathbf{r})$ with the limit of uniform density being taken after taking the functional derivative two times, so the extended form of Eq. (18) for nonuniform polymers takes into account the main term of the expansion correctly. (iii) The closure equation (25) for the PRISM integral equation is completely identical to that for the OZ equation (as can be seen in our recent paper [34]). Equation (18) (or its mixture form) can be derived from Eq. (25) (or its mixture form) by making use of the reversibility of the derivation in the Appendix, the universality of the free-energy density functional, and the OZ equation (or its mixture form). Now if we want to derive the extended form of Eq. (18) from Eq. (25), in order to arrive at the correct second term in the extended form of Eq. (18), we have to replace $h-C_0^{(2)}$ by the OZ equation, not the PRISM equation, so the argument of B in the extended form of Eq. (18) should be the same as the second term in the same equation as Eq. (18).

However, it should be pointed out that by ''the main expansion term'' we mean that it determines general properties of the final prediction, for example the basic shape of the density distribution curve, and by ''the residue term'' we mean that it is small in absolute value compared with ''the main expansion term,'' so it does not have a great effect on the general shape of the density distribution curve. But it includes rich and detailed information on the shape of the density distribution curve (for example, the contact density, the amplitude of the trough, the wave crest, etc.), so its incorporation in the extended form of Eq. (18) will improve on the accuracy of the prediction greatly (as will be displayed in the latter part of the paper). This has been the case for nonuniform hard sphere fluids [29] in which the prediction accuracy is greatly improved on due to the incorporation of ''the residue term.''

Substituting Eqs. (16)–(18) into Eq. (15) yields

$$\rho_p(\mathbf{R})=\rho_p^b \exp\Bigg\{-\beta\sum_{i=1}^{N_p}\varphi_{\rm ext}(\mathbf{r}_i)-\beta V_p(\mathbf{R}) +\sum_{i=1}^{N_p}\int[\rho(\mathbf{r}')-\rho^b]C_0^{(2)}C_0^{(2)}(|\mathbf{r}_i-\mathbf{r}'|;\rho^b)d\mathbf{r}' +B\Bigg[\int[\rho(\mathbf{r}')-\rho^b]C_0^{(2)}(|\mathbf{r}_i-\mathbf{r}'|;\rho^b)d\mathbf{r}'\Bigg]\Bigg\}. \tag{26}$$

From Eqs. (1) and (2), one obtains

$$\exp(-1/kTV_p(\mathbf{R}))=\prod_{i=1}^{N_p-1}k_c\delta(|\mathbf{r}_{i+1}-\mathbf{r}_i|-\sigma), \tag{27}$$

where k_c is a constant whose value will be determined lately by analyzing the case in which the effect of the external potential is negligible.

Substituting Eqs. (26) and (27) into Eq. (8) leads to

$$\begin{aligned}\rho(\mathbf{r})=&\int d\mathbf{r}_1\int d\mathbf{r}_2\cdots\int d\mathbf{r}_{N_p}\sum_{i=1}^{N_p}\delta(\mathbf{r}-\mathbf{r}_i)\rho_p^b F\\ &\times[-\beta\varphi_{\rm ext}(\mathbf{r}_i),\rho(\mathbf{r}_i)]\prod_{j=1,\neq i}^{N_p}F[-\beta\varphi_{\rm ext}(\mathbf{r}_j),\rho(\mathbf{r}_j)]\\ &\times\prod_{k=i}^{2}k_c\delta(|\mathbf{r}_{k-1}-\mathbf{r}_k|-\sigma)\prod_{k=i}^{N_p-1}k_c\delta(|\mathbf{r}_{k+1}-\mathbf{r}_k|-\sigma)\\ =&\rho_p^b F[-\beta\varphi_{\rm ext}(\mathbf{r}),\rho(\mathbf{r})]\sum_{i=1}^{N_p}\int d\mathbf{r}_{i-1}\int d\mathbf{r}_{i-2}\cdots\int d\mathbf{r}_1\\ &\times\prod_{k=i,\mathbf{r}_i\equiv\mathbf{r}}^{2}k_c\delta(|\mathbf{r}_{k-1}-\mathbf{r}_k|-\sigma)\\ &\times\prod_{k=1}^{i-1}F[-\beta\varphi_{\rm ext}(\mathbf{r}_k),\rho(\mathbf{r}_k)]\\ &\times\int d\mathbf{r}_{i+1}\int d\mathbf{r}_{i+2}\cdots\int d\mathbf{r}_{N_p}\prod_{k=i,\mathbf{r}_i\equiv\mathbf{r}}^{N_p-1}k_c\delta\\ &\times(|\mathbf{r}_{k+1}-\mathbf{r}_k|-\sigma)\prod_{k=i+1}^{N_p}F[-\beta\varphi_{\rm ext}(\mathbf{r}_k),\rho(\mathbf{r}_k)],\end{aligned} \tag{28}$$

where

$$F[-\beta\varphi_{\mathrm{ext}}(\mathbf{r}),\rho(\mathbf{r})]=\exp\Bigg\{-\beta\varphi_{\mathrm{ext}}(\mathbf{r})+\int[\rho(\mathbf{r}')-\rho^b]C_0^{(2)}\times(|\mathbf{r}-\mathbf{r}'|;\rho^b)d\mathbf{r}'+B\Bigg[\int[\rho(\mathbf{r}')-\rho^b]\times C_0^{(2)}(|\mathbf{r}-\mathbf{r}'|;\rho^b)d\mathbf{r}'\Bigg]. \tag{29}$$

Equations (28) and (29), which can be solved only numerically, provide the polymer site density profile under the site external potential $\varphi_{\mathrm{ext}}(\mathbf{r})$.

B. Numerical solution

To solve Eqs. (28) and (29), one must first solve the PRISM equation (24) coupled with the closure equation (25) and the PY bridge function equation (21). Following the method used for solving the OZ equation, we rewrite the PRISM equation (24) in the Fourier space as

$$\hat{h}(k)=\hat{w}(k)\hat{C}_0^{(2)}(k;\rho^b)\hat{w}(k)+\rho^b\hat{w}(k)\hat{C}_0^{(2)}(k;\rho^b)\hat{h}(k), \tag{30}$$

where carets denote the Fourier transform, which is defined, for example for $h(r)$, as

$$\hat{h}(k)=\frac{4\pi}{k}\int_0^\infty rh(r)\sin(kr)dr. \tag{31}$$

Equation (30) can be rearranged in the following form suitable for iteration:

$$\hat{\gamma}(k)=\frac{\hat{C}_0^{(2)}(k;\rho^b)[\hat{w}^2(k)-1]+\rho^b\hat{w}(k)\hat{C}_0^{(2)^2}(k;\rho^b)}{1-\rho^b\hat{w}(k)\hat{C}_0^{(2)}(k;\rho^b)}. \tag{32}$$

The closure equation (25) is rewritten as

$$C_0^{(2)}(r;\rho^b)=\exp(-\beta\phi(r)+\gamma(r)+B(r))-\gamma(r)-1, \tag{33}$$

where $\phi(r)$ is the hard sphere pair potential,

$$\phi(r)=\infty,\quad r<\sigma$$
$$=0,\quad r>\sigma. \tag{34}$$

The basic iterative strategy is as follows: One assumes $\gamma(r)$, one calculates $C_0^{(2)}(r;\rho^b)$ using Eq. (33), $C_0^{(2)}(r;\rho^b)$ is then Fourier transformed to get $\hat{C}_0^{(2)}(k;\rho^b)$, one calculates $\hat{\gamma}(k)$ using Eq. (32), $\hat{\gamma}(k)$ is Fourier transformed back to get $\gamma(r)$; the above steps are repeated until convergence. To accelerate the convergence, one can use the algorithm by Labik *et al.* [35] to solve the OZ equation, which is an extension of Gillan's algorithm [36]. The approximate single-chain structure factor $\hat{w}(k)$ is first determined from the Koyama distribution [37] for a semiflexible hard sphere chain with the energy parameter being forced to be zero (when the energy parameter is zero, the semiflexible hard sphere chain becomes a freely jointed hard sphere chain).

Equation (28) can be simplified by making use of the properties of the Dirac δ function. After some manipulations, Eq. (28) becomes

$$\rho(\mathbf{r})=\rho_p^bF[-\beta\varphi_{\mathrm{ext}}(\mathbf{r}),\rho(\mathbf{r})]\sum_{i=1}^{N_p}F_i[-\beta\varphi_{\mathrm{ext}}(\mathbf{r}),\rho(\mathbf{r})]\times F_{N_p+1-i}[-\beta\varphi_{\mathrm{ext}}(\mathbf{r}),\rho(\mathbf{r})], \tag{35}$$

where

$$F_n[-\beta\varphi_{\mathrm{ext}}(\mathbf{r}),\rho(\mathbf{r})]=\int_0^{2\pi}d\theta\int_0^{\pi}d\phi\sin(\phi)F[-\beta\varphi_{\mathrm{ext}}(\mathbf{r}+\mathbf{I}),\times\rho(\mathbf{r}+\mathbf{I})F_{n-1}[-\beta\varphi_{\mathrm{ext}}(\mathbf{r}+\mathbf{I}),\rho(\mathbf{r}+\mathbf{I})]. \tag{36}$$

$\mathbf{I}=(\sin\phi\cos\theta,\sin\phi\sin\theta,\cos\phi)$ is an arbitrary unit vector, and $F_1[-\beta\varphi_{\mathrm{ext}}(\mathbf{r}),\rho(\mathbf{r})]=1$.

Equation (36) can be further simplified for symmetrical cases, for example when the external potential is spherically symmetrical, that is, $\varphi_{\mathrm{ext}}(\mathbf{r})=\varphi_{\mathrm{ext}}(\mathbf{r})$. Then,

$$F_n[-\beta\varphi_{\mathrm{ext}}(r),\rho(r)]=2\pi\int_0^{\pi}d\phi\sin\phi F\times[-\beta\varphi_{\mathrm{ext}}(\sqrt{1+r^2+2r\cos\phi}),\times\rho(\sqrt{1+r^2+2r\cos\phi})]F_{n-1}\times[-\beta\varphi_{\mathrm{ext}}(\sqrt{1+r^2+2r\cos\phi}),\times\rho(\sqrt{1+r^2+2r\cos\sigma})]. \tag{37}$$

When the external potential is due to one or two parallel walls, that is, $\varphi_{\mathrm{ext}}(\mathbf{r})=\varphi_{\mathrm{ext}}(z)$, then

$$F_n[-\beta\varphi_{\mathrm{ext}}(z),\rho(z)]=2\pi\int_0^{\pi}d\phi\sin\phi F\times[-\beta\varphi_{\mathrm{ext}}(\sqrt{z+\cos\phi}),\times\rho(\sqrt{z+\cos\phi})]F_{n-1}\times[-\beta\varphi_{\mathrm{ext}}(\sqrt{z+\cos\phi}),\times\rho(\sqrt{z+\cos\phi})]. \tag{38}$$

Let us now consider the region outside the range of action of the external potential, that is, the region where the average local site density distribution is constant and equal to ρ^b. Then, $F[-\beta\varphi_{\mathrm{ext}}(\mathbf{r}),\rho(\mathbf{r})]$ becomes equal to 1, and all $F_n[-\beta\varphi_{\mathrm{ext}}(\mathbf{r}),\rho(\mathbf{r})]$ are equal to $k_c4\pi$ except $F_1[-\beta\varphi_{\mathrm{ext}}(\mathbf{r}),\rho(\mathbf{r})]$, which is equal to 1. Consequently,

$$\rho^b = \rho_p^b[2k_c 4\pi + (N_p - 2)(k_c 4\pi)^2], \tag{39}$$

thus k_c should be equal to $1/4\pi$.

It should be pointed out that one previous paper [38] also achieved the same simplification of avoiding the use of the single-chain Monte Carlo simulation for two cases, namely the freely jointed hard sphere chain and the Gaussian chain. In Ref. [38], the final coupled integral equations are similar in form to Edwards-Helfand-Tagami ''self-consistent-field'' theory, and their ''medium-induced potential'' is only the polymer analog of the HNC approximation employed in liquid state theories of atomic fluids. In the present paper, the same simplification was achieved in the basic DFT framework itself. It is not necessary to resort to the concept of field theory, so its derivation is enormously simplified compared with that in Refs. [38] and [39]. Furthermore, the present paper goes beyond the simple HNC approximation, and includes all expansion terms beyond the second order in the form of a bridge function. By comparing the present Eq. (18) with Eq. (24) in Ref. [38], we find that the medium-induced potential in Refs. [38] and [39] is actually the deviation of the excess chemical potential for a nonuniform fluid from the excess chemical potential for the corresponding uniform fluid. Thus, by the present derivation, we disclose the physical content of the concept of the medium-induced potential in the self-consistent-field theory and build the bridge between the self-consistent-field theory and density-functional theory. Also with the concept of a bridge function, we propose a systematic methodology to improve upon the treatment of the medium-induced potential in the self-consistent-field theory.

Equation (28) can be solved iteratively. By selecting $\rho(\mathbf{r})$ and calculating $F[-\beta\varphi_{\text{ext}}(\mathbf{r}),\rho(\mathbf{r})]$ and $F_n[-\beta\varphi_{\text{ext}}(\mathbf{r}),\rho(\mathbf{r})]$ for $n=2,3,...,N_p$ using Eqs. (29) and (36), respectively, coupled with the numerical solution of $C_0^{(2)}(r;\rho^b)$, and then calculating a new $\rho(\mathbf{r})$ using Eq. (35), the above steps are repeated until convergence. To prevent divergence, it is necessary to mix new and old $\rho(\mathbf{r})$ in certain proportions. Regarding the choice of bridge function appearing in Eq. (18), we find that as with the case of a nonuniform hard sphere fluid [29], the results based on the VM bridge function are more accurate than those based on the PY bridge function for all cases calculated in the present paper. For this reason, the reported data in the present paper are all based on the VM bridge function.

III. COMPARISON WITH SIMULATIONS AND OTHER APPROACHES

In the present paper, we consider two cases: in one, the external potential is due to a planar hard wall, and in the other, it is due to two planar hard walls at a separation $H\sigma$. In the first case, the local site density distribution is denoted by $\rho_{ow}(z)$ and the external potential has the form

$$\begin{aligned} \phi_{\text{ext}}(z) &= \infty, \quad z<0, \\ &= 0, \quad z>0. \end{aligned} \tag{40}$$

In the second case, the local site density distribution is denoted by $\rho(z)$ and the external potential has the form

$$\begin{aligned} \phi_{\text{ext}}(z) &= \infty, \quad z<0 \ \text{ or } \ z>H\sigma, \\ &= 0, \quad \text{otherwise}. \end{aligned} \tag{41}$$

After the local site density distribution is determined, all other quantities can be calculated from it. In the present paper, we calculate the adsorption isotherms for hard chains between two hard walls at separation $H\sigma$, expressed as the average site volume fraction η_{av},

$$\eta_{\text{av}} = \frac{\pi}{6H}\int_0^H \rho(z)dz, \tag{42}$$

as well as the partition coefficient K_c defined as

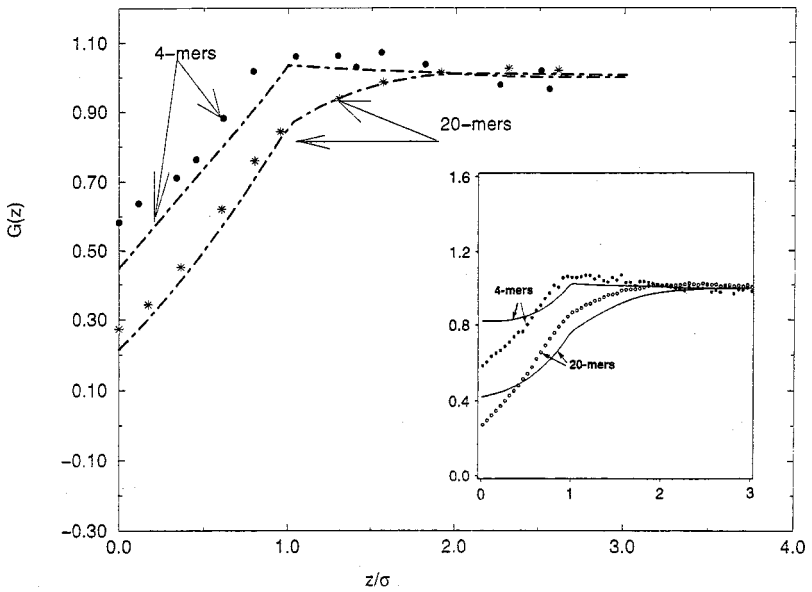

FIG. 1. The normalized density distribution profile for 4- and 20-mers near a hard wall for a bulk site volume fraction $\eta^b=0.1$. The symbols represent simulation results [41,42] and the lines represent the theoretical predictions. The inset contains the predictions of Ref. [7] and the corresponding simulation results.

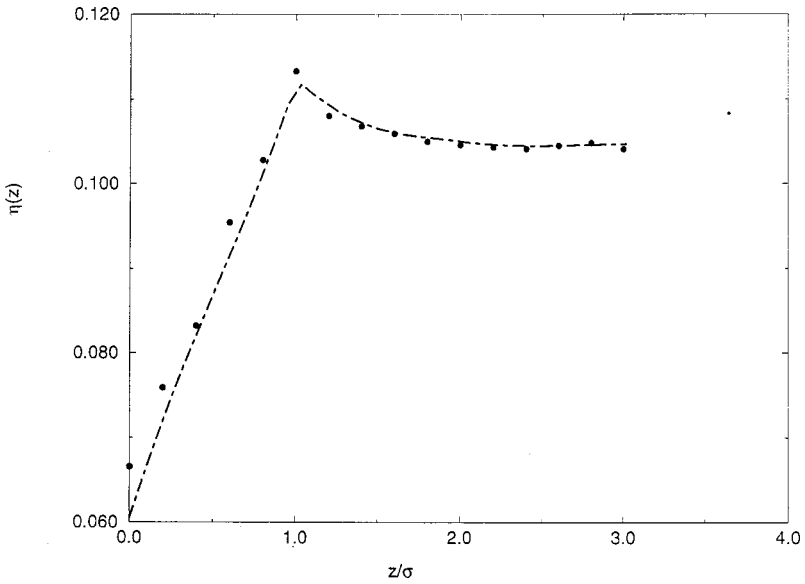

FIG. 2. The site volume fraction distribution profile for 3-mers between two hard walls for a separation $H=10\sigma$ and an average site volume fraction $\eta_{\mathrm{av}}=0.1$. The symbols represent the simulation results [43] and the lines represent the theoretical predictions.

$$K_c=\frac{\eta_{av}}{\eta^b}, \tag{43}$$

where $\eta^b=(\pi/6)\rho^b$ is the bulk site volume fraction.

The pressure acting on the inside faces of the two hard walls is given by [40]

$$\beta P_{\mathrm{inside}}=\rho(\sigma/2), \tag{44}$$

while that acting on the outside faces, which is equal to the bulk pressure, is given by

$$\beta P_{\mathrm{bulk}}=\rho_{ow}(\sigma/2). \tag{45}$$

Consequently, the medium-induced force per unit area f is the difference

$$f=\beta P_{\mathrm{inside}}-\beta P_{\mathrm{bulk}}. \tag{46}$$

Let us now compare the predictions of the present theory with the computer-simulation results and those of the previous theories. The cases of 4- and 20-mers near one hard wall at the low bulk site volume fraction $\eta^b=0.1$ are presented in Fig. 1, where the ordinate is the normalized density distribution $G(z)=\rho_{ow}(z)\pi/6\eta^b$. Figure 1 shows that the present theory predicts the surface depletion correctly, and that the present agreement with simulation data is better than that of Ref. [7]. The surface depletion occurs when the bulk density is low, because the entropic penalty effect dominates in this case over the packing effect. The density distributions for the case of 3-mers between two hard walls at the average site volume fractions of 0.1, 0.3, and 0.4 are presented in Figs. 2–4, respectively, and those for 20-mers between two hard walls at the average site volume fractions of 0.1 and 0.45 are in Figs. 5 and 6, respectively. The Monte Carlo density-functional theory of Ref. [23] is regarded as the most accurate theory for polymers at surfaces in Ref. [24]. Reference

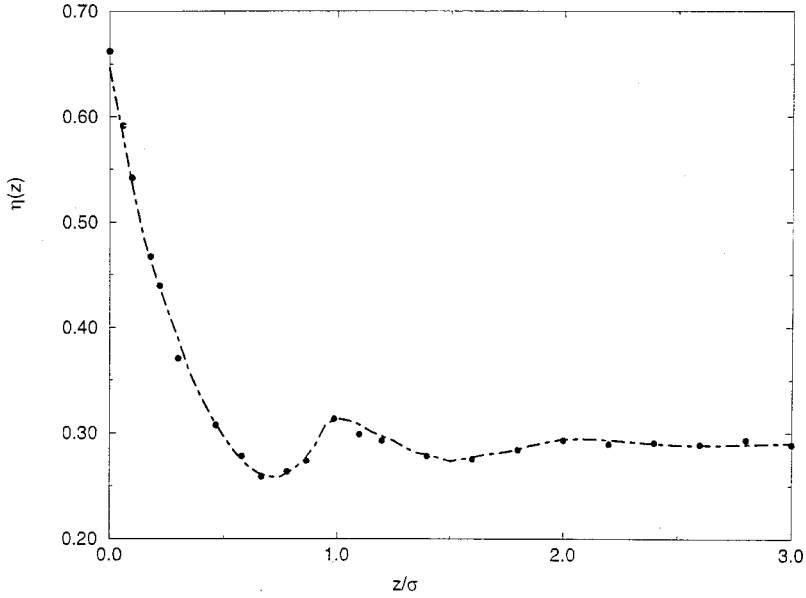

FIG. 3. The same as in Fig. 2, but with an average site volume fraction $\eta_{\mathrm{av}}=0.3$.

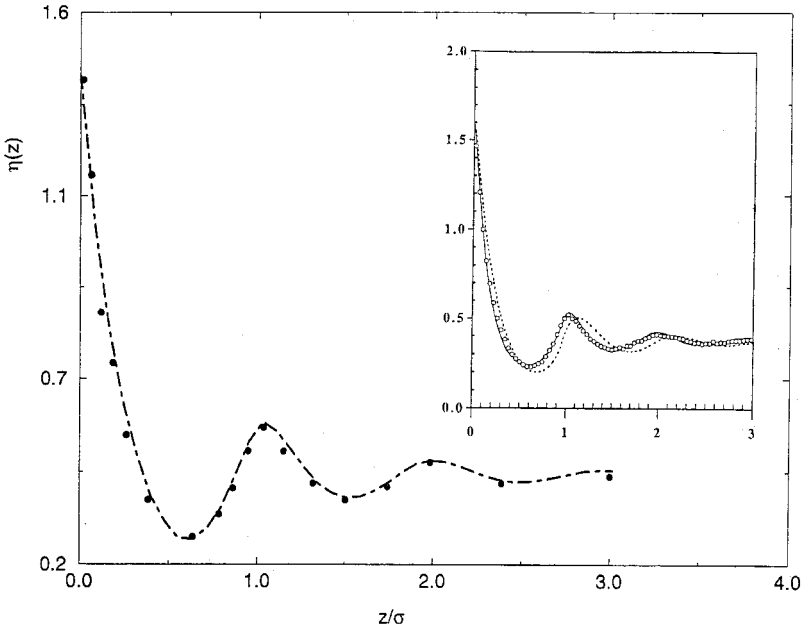

FIG. 4. The same as in Fig. 2, but with an average site volume fraction $\eta_{av}=0.4$. In the inset, the solid line represents the predictions of the Monte Carlo density-functional theory of Ref. [24], the dotted line the predictions of the Monte Carlo density-functional theory of Ref. [23], and the symbols the simulation data [43].

[24] improved upon the theory of Ref. [23] by treating the excess part of free energy of nonuniform polymer melts with a Curtin-Ashcroft-type weighted-density approximation, but still using the single-chain simulation to treat the corresponding ideal part as in Ref. [23]. Because the ideal part is treated accurately by the single-chain simulation in both theories [23,24] and the ideal part dominates when the bulk density is low, the predictions of both theories provide the same accuracy at low density. At high density, the predictions of Ref. [24] are more accurate than those of Ref. [23]. To compare with these theories, the predictions of Refs. [23], [24] are displayed in the insets of Figs. 4 and 6. Figures 2–6 show that our theory correctly predicts the transition from surface depletion at low density to surface enhancement at high density. It is even somewhat more accurate than the theory of Ref. [24]. Both the present theory and that of Ref. [24] are more accurate than that of Ref. [23] at high densities, and the three theories have almost the same accuracy at low densities. Figures 7 and 8 present the partition coefficient and the average site volume fraction versus the bulk site volume fraction and the bulk pressure, respectively, for the cases of 4- and 8-mers. The predictions of the integral equation theory of Ref. [7] are displayed in the insets of Figs. 7 and 8. These two figures show that the present theory and that of Ref. [7] are in agreement with simulation data. Equation (46) allows one to calculate the medium-induced force per unit area f as a function of wall separation H. As an example, f is plotted against H in Figs. 9 and 10 for, respectively, 8- and 4-mers polymer melts confined between two hard walls at several bulk site volume fractions. These figures show that at low bulk site volume fractions, the oscillations are weak and the force becomes attractive at short separations. As the bulk site volume fraction increases, the amplitude of the oscillations increases, the attractive force disappears, being re-

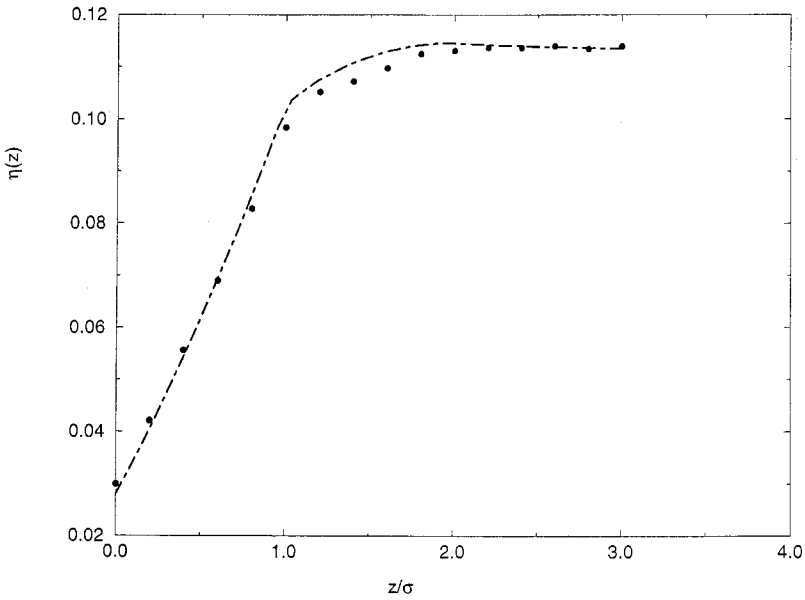

FIG. 5. The site volume fraction distribution profile for a 20-mer between two hard walls for a separation $H=10\sigma$ and an average site volume fraction $\eta_{av}=0.1$. The symbols represent the simulation results [44] and the lines represent the theoretical predictions.

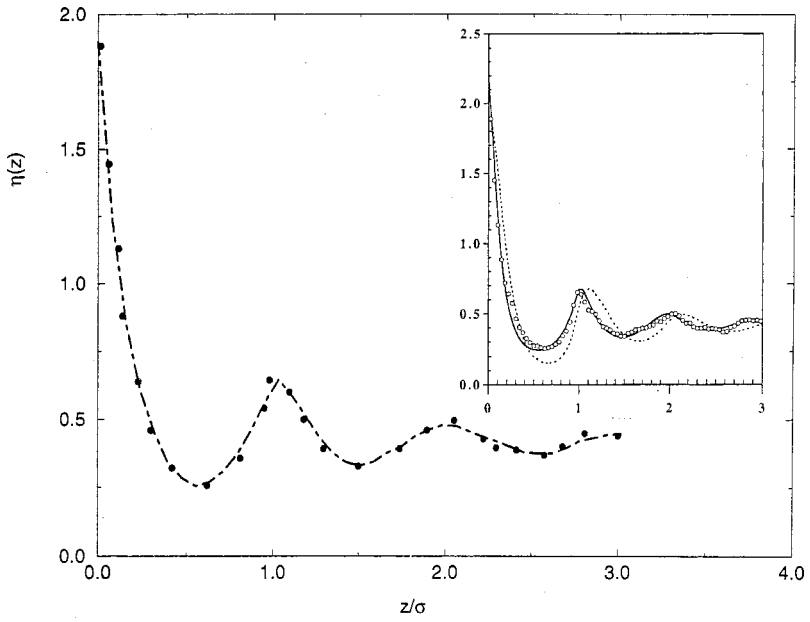

FIG. 6. The same as in Fig. 5, but with an average site volume fraction $\eta_{av}=0.45$. In the inset, the solid line represents the predictions of the Monte Carlo density-functional theory of Ref. [24], the dotted line the predictions of the Monte Carlo density-functional theory of Ref. [23], and the symbols the simulation data [24].

placed by a strong repulsiveness at short separations and high bulk site volume fractions. For the same bulk site volume fraction, a smaller number of segments induces oscillations and repulsiveness, but a larger number of segments inhibits oscillations and induces attractiveness. One can also see that the period of oscillations is approximately one unit diameter. The predicted oscillations at high bulk site volume fraction are in agreement with the experimental observations of Israelachvili and co-workers [45,46] made with the surface force apparatus. It is, however, impossible to compare quantitatively the predictions of the present theory with the experimental data of Israelachvili and co-workers because they employed a mixture of polymers.

IV. CONCLUDING REMARKS

In summary, a density-functional theory for nonuniform polymer melts was proposed, which has the same accuracy as, or even greater accuracy than, the previous two most accurate Monte Carlo density-functional theories [23,24] and more accurate than the integral equation theory [7]. It is computationally modest due to the fact that the properties of the Dirac δ function could be used to simplify the treatment of the connectivity of monomers in the chain, thus avoiding the use of the single-chain simulation to calculate the ideal free-energy contribution. It should be noted that a recent interesting paper [49] proposed a methodology that permitted one to take the single-chain Monte Carlo simulation out of the iterative loop and to investigate different cases from a single Monte Carlo simulation. However, the ''medium-induced potential'' in Refs. [38], [39], [49] is of the HNC approximation type, the present paper relates the medium-induced potential to the deviation of the excess chemical potential for nonuniform fluid from the excess chemical potential for the corresponding uniform fluid, and systemati-

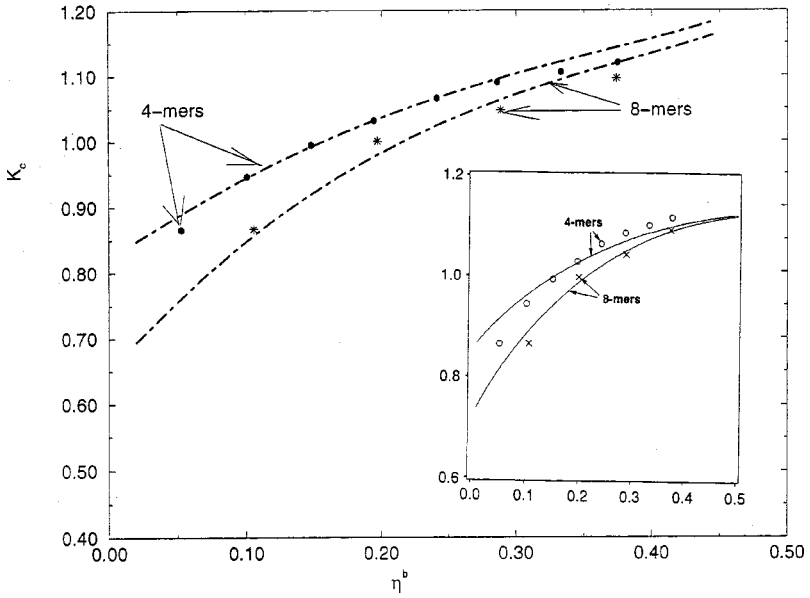

FIG. 7. Variation of the partition coefficient K_c with the bulk site volume fraction η^b for 4- and 8-mers and $H=5\sigma$. The symbols represent the simulation results [42] and the lines represent the theoretical predictions. In the inset, the lines represent the predictions of the integral equation theory of Ref. [7] and the symbols represent the corresponding simulation data [42].

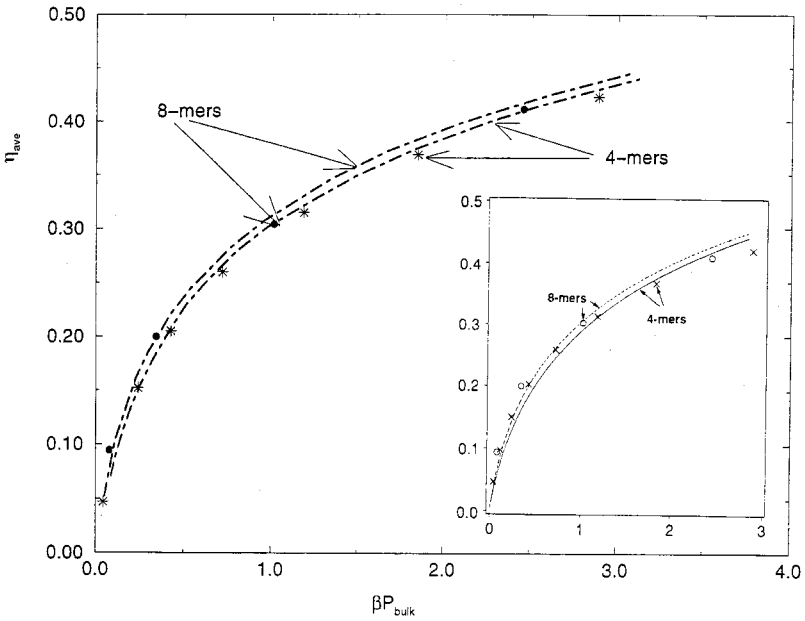

FIG. 8. Variation of the average site volume fraction η_{av} with the bulk pressure βP_{bulk} for 4- and 8-mers and $H=5\sigma$. The symbols represent the simulation results [42] and the lines represent the theoretical predictions. In the inset, the lines represent the predictions of the integral equation theory of Ref. [7] and the symbols represent the corresponding simulation data [42].

cally improves the medium-induced potential by the bridge function conception. The present theory treats the excess free-energy contribution by making use of the universality of the free-energy density functional, hence the present formulation of DFT is completely different from the previous versions of DFT, which treat the excess free-energy contribution by using various versions of the weighted-density approximation [6,15,23,24] or of the perturbative expansion [12–14]. The extension to mixtures of nonuniform polymers and to nonuniform polyelectrolytes will be reported in a forthcoming paper.

APPENDIX

To derive Eq. (18), it is convenient to expand $C^{(1)}(\mathbf{r};[\rho(\mathbf{r})])$ around the uniform system of bulk density ρ^b as follows:

$$C^{(1)}(\mathbf{r};[\rho\mathbf{r}]) = C_0^{(1)}(\rho^b) + \int d\mathbf{r}_1[\rho(\mathbf{r}_1)-\rho^b]C_0^{(2)}(|\mathbf{r}-\mathbf{r}_1|;\rho^b) + \sum_{n=3}^{\infty}\frac{1}{(n-1)!}\int d\mathbf{r}_1\int d\mathbf{r}_2\cdots\int d\mathbf{r}_{n-1} \times\prod_{m=1}^{n-1}[\rho(\mathbf{r}_m)-\rho^b]C_0^{(n)}(\mathbf{r},\mathbf{r}_1,\ldots,\mathbf{r}_{n-1};\rho^b), \quad \text{(A1)}$$

where $C_0^{(n)}(\mathbf{r},\mathbf{r}_1,\ldots,\mathbf{r}_{n-1};\rho^b)$ is the nth-order direct correlation function (DCF) of a uniform system of bulk density ρ^b.

Even in a uniform system, there is a nonuniform density profile around each molecule located in the origin given by [47]

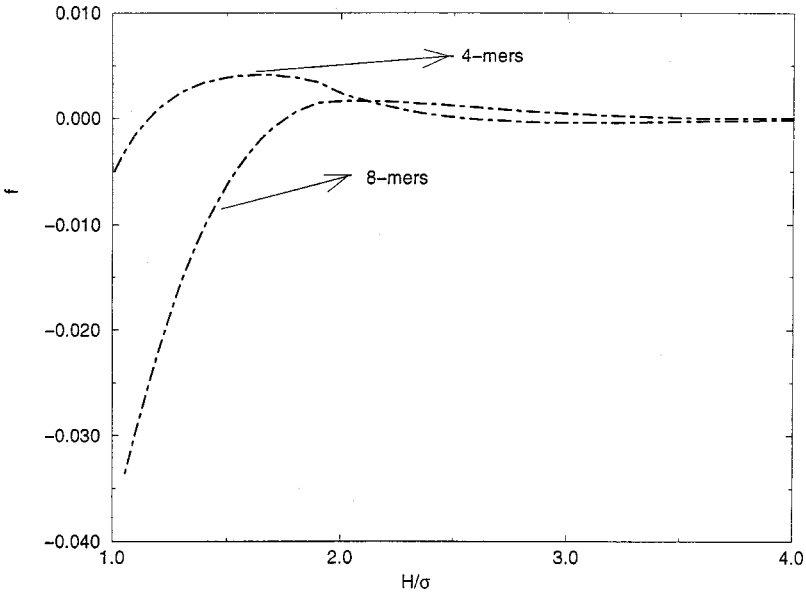

FIG. 9. Variation of the medium-induced force per unit area f with the wall separation H/σ for 4- and 8-mers and $\eta^b=0.1$.

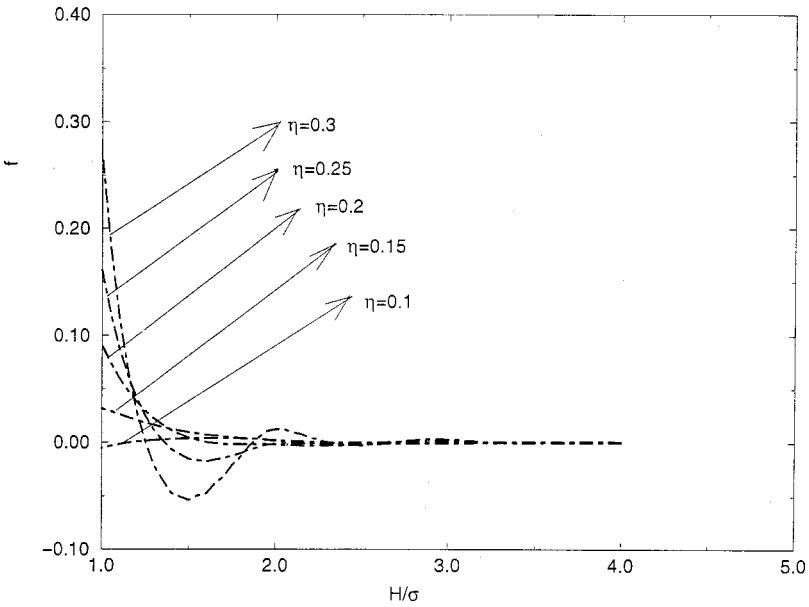

FIG. 10. Variation of the medium-induced force per unit area f with the wall separation H/σ for 4-mers and various values of η^b.

$$\rho(\mathbf{r}) = \rho^b g(\mathbf{r}), \tag{A2}$$

where $g(\mathbf{r})$ is the radial distribution function of the bulk fluid. Thus, for this special type of inhomogeneity, Eq. (A1) acquires the following form:

$$C^{(1)}(\mathbf{r};[\rho^b g(\mathbf{r})]) = C_0^{(1)}(\rho^b) + \int d\mathbf{r}_1[\rho^b g(\mathbf{r}_1) - \rho^b] C_0^{(2)}(|\mathbf{r} - \mathbf{r}_1|;\rho^b) + \sum_{n=3}^{\infty} \frac{\rho^{b(n-1)}}{(n-1)!} \times \int d\mathbf{r}_1 \int d\mathbf{r}_2 \cdots \int d\mathbf{r}_{n-1} \times \prod_{m=1}^{n-1} h(\mathbf{r}_m) C_0^{(n)}(\mathbf{r}, \mathbf{r}_1, \ldots, \mathbf{r}_{n-1};\rho^b), \tag{A3}$$

where $h(\mathbf{r}) = g(\mathbf{r}) - 1$ is the total correlation function of the bulk fluid. The third term in the right-hand side of the above equation represents the bridge function [48], which will be denoted as $B[\vartheta(\mathbf{r})]$. The bridge function can be expressed as a functional of a correlation function, such as the radial distribution function $g(\mathbf{r})$, the second-order direct correlation function $C_0^{(2)}(r;\rho^b)$, the cavity correlation function $y(\mathbf{r})$, the indirect correlation function $\gamma(\mathbf{r})$, or any of these combinations. Consequently, Eq. (A3) can be rewritten as

$$C^{(1)}(\mathbf{r};[\rho^b g(\mathbf{r})]) = C_0^{(1)}(\rho^b) + \int d\mathbf{r}_1[\rho^b g(\mathbf{r}_1) - \rho^b] C_0^{(2)} \times (|\mathbf{r} - \mathbf{r}_1|;\rho^b) + B[\vartheta(\mathbf{r})]. \tag{A4}$$

Because the functional $F_{\mathrm{ex}}(\mathbf{r};[\rho(\mathbf{r})])$ [hence $C^{(1)}(\mathbf{r};[\rho(\mathbf{r})]) = -\beta\delta F_{\mathrm{ex}}(\mathbf{r};[\rho(\mathbf{r})])/\delta\rho(\mathbf{r})$, its functional derivative with respective to $\rho(\mathbf{r})$] is, for a given interaction potential, a universal functional [50] of the density distribution $\rho(\mathbf{r})$ and is independent of the external potential responsible for the generation of the density distribution $\rho(\mathbf{r})$. Thus, we can specify the functional form of $C^{(1)}(\mathbf{r};[\rho(\mathbf{r})])$ by a specific case where the external potential is the interaction potential between a particle situated in the origin and the bulk particles. One therefore can conclude that $C^{(1)}(\mathbf{r};[\rho(\mathbf{r})])$ for a general nonuniform system has the same form as Eq. (A4). Let us recall that $\rho(\mathbf{r})$ was replaced by $\rho^b g(\mathbf{r})$ for the special inhomogeneity that provided Eqs. (A3) and (A4). It is clear that for a general nonuniform system, $g(\mathbf{r})$ in Eq. (A4) should be replaced by $\rho(\mathbf{r})/\rho^b$. Consequently, the following form for $C^{(1)}(\mathbf{r};[\rho(\mathbf{r})])$ for a general nonuniform system is obtained:

$$C^{(1)}(\mathbf{r};[\rho(\mathbf{r})]) = C_0^{(1)}(\rho^b) + \int d\mathbf{r}_1[\rho(\mathbf{r}_1) - \rho^b] C_0^{(2)} \times (|\mathbf{r} - \mathbf{r}_1|;\rho^b) + B[\vartheta(\mathbf{r})]. \tag{A5}$$

In Ref. [29], $\vartheta(\mathbf{r})$ was chosen to be the indirect correlation function $\gamma(\mathbf{r})$. However, the Ornstein-Zernike (OZ) equation

$$h(r) = C_0^{(2)}(r;\rho^b) + \rho^b \int d\mathbf{r}_1 h(\mathbf{r}_1) C_0^{(2)}(|\mathbf{r} - \mathbf{r}_1|;\rho^b) \tag{A6}$$

indicates that $\gamma(\mathbf{r})$ can be replaced by $\rho^b \int d\mathbf{r}_1 h(\mathbf{r}_1) C_0^{(2)}(|\mathbf{r} - \mathbf{r}_1|;\rho^b)$. Of course, $g(\mathbf{r}) = h(\mathbf{r}) + 1$ should be replaced in the above expression by $\rho(\mathbf{r})/\rho^b$. Thus one arrives at Eq. (18) in the text.

[1] H. K. Christenson, D. W. R. Gruen, R. G. Horn, and J. N. Israelachvili, J. Chem. Phys. **87**, 1834 (1987).
[2] C. Allain, D. Ausserre, and F. Rondelez, Phys. Rev. Lett. **49**, 1694 (1982).
[3] D. H. Napper, *Polymeric Stabilization of Colloidal Dispersions* (Academic, London, 1983).
[4] P. G. DeGennes, *Scaling Concepts in Polymer Physics* (Cornell University Press, Ithaca, NY, 1979).
[5] J. M. H. M. Scheutjens and G. J. Fleer, J. Phys. Chem. **83**, 1619 (1979); **84**, 1882 (1980).
[6] M. Bjorling and P. Linse, J. Chem. Phys. **97**, 6890 (1992).
[7] A. Yethiraj and C. K. Hall, J. Chem. Phys. **95**, 3749 (1991).
[8] J. G. Curro and K. S. Schweizer, J. Chem. Phys. **87**, 1842 (1987).
[9] D. Henderson, F. F. Abraham, and J. A. Barker, Mol. Phys. **31**, 1291 (1975).
[10] Y. Zhou and G. Stell, Mol. Phys. **66**, 767 (1989).
[11] H. Nakanishi and P. Pincu, J. Chem. Phys. **79**, 997 (1983).
[12] D. Chandler, J. D. McCoy, and S. J. Singer, J. Chem. Phys. **85**, 5971 (1986).
[13] D. Chandler, J. D. McCoy, and S. J. Singer, J. Chem. Phys. **85**, 5977 (1986).
[14] W. E. McMullen and K. F. Freed, J. Chem. Phys. **92**, 1413 (1990).
[15] C. E. Woodward, J. Chem. Phys. **94**, 3183 (1991).
[16] E. Kierlik and M. L. Rosinberg, J. Chem. Phys. **97**, 9222 (1992).
[17] E. Kierlik and M. L. Rosinberg, J. Chem. Phys. **99**, 3950 (1993).
[18] E. Kierlik and M. L. Rosinberg, J. Chem. Phys. **100**, 1716 (1994).
[19] M. S. Wertheim, J. Stat. Phys. **35**, 19 (1984).
[20] M. S. Wertheim, J. Stat. Phys. **35**, 35 (1984).
[21] M. S. Wertheim, J. Stat. Phys. **42**, 459 (1986).
[22] M. S. Wertheim, J. Stat. Phys. **42**, 477 (1986).
[23] A. Yethiraj and C. E. Woodward, J. Chem. Phys. **102**, 5499 (1995).
[24] A. Yethiraj, J. Chem. Phys. **109**, 3269 (1998).
[25] A. Yethiraj and C. K. Hall, J. Chem. Phys. **91**, 4827 (1989).
[26] I. Bitsanis and G. Hadziioannou, J. Chem. Phys. **92**, 3827 (1990).
[27] S. Sen, J. D. McCoy, S. K. Nath, J. P. Donley, and J. G. Curro, J. Chem. Phys. **102**, 3431 (1995).
[28] J. P. Hansen and I. R. McDonald, *Theory of Simple Liquids* (Academic, New York, 1986).
[29] S. Zhou and E. Ruckenstein, J. Chem. Phys. **112**, 8079 (2000).
[30] J. K. Percus and G. J. Yevick, Phys. Rev. **110**, 1 (1958).
[31] L. Verlet, Mol. Phys. **41**, 183 (1980).
[32] D. Chandler, in *The Liquid State of Matter: Fluids, Simple and Complex*, edited by E. W. Montroll and J. L. Lebowitz (North Holland, Amsterdam, 1982).
[33] A. Yethiraj and K. S. Schweizer, J. Chem. Phys. **97**, 1455 (1992).
[34] S. Zhou, J. Chem. Phys. **113**, 8719 (2000).
[35] S. Labik, A. Malijevsky, and P. Vonka, Mol. Phys. **56**, 709 (1985).
[36] M. J. Gillan, Mol. Phys. **38**, 1781 (1979).
[37] K. G. Honnell, J. G. Curro, and K. S. Schweizer, Macromolecules **23**, 3496 (1990).
[38] J. P. Donley, J. J. Rajasekaran, J. D. McCoy, and J. G. Curro, J. Chem. Phys. **103**, 5061 (1995).
[39] J. P. Donley, J. G. Curro, and J. D. McCoy, J. Chem. Phys. **101**, 3205 (1994).
[40] R. Dickman and C. K. Hall, J. Chem. Phys. **89**, 3168 (1988).
[41] A. Yethiraj and C. K. Hall, Macromolecules **23**, 1865 (1990).
[42] A. Yethiraj and C. K. Hall, Mol. Phys. **73**, 3 (1991).
[43] S. Phan, M. L. Rosinberg, E. Kierlik, A. Yethiraj, and R. Dickman, J. Chem. Phys. **102**, 2141 (1995).
[44] A. Yethiraj, J. Chem. Phys. **101**, 2489 (1994).
[45] M. L. Gee and J. N. Israelachvili, J. Chem. Soc., Faraday Trans. **86**, 4049 (1990).
[46] J. N. Israelachvili and S. J. Kott, J. Chem. Phys. **88**, 7162 (1988).
[47] J. K. Percus, in *The Equilibrium Theory of Classical Fluids*, edited by H. L. Frisch and A. L. Lebowitz (Benjamin, New York, 1964), p. 113.
[48] H. Iyetomi, Prog. Theor. Phys. **71**, 427 (1984).
[49] J. B. Hooper, J. D. McCoy, and J. G. Curro, J. Chem. Phys. **112**, 3090 (2000).
[50] J. T. Chayes, L. Chayes, Commun. Math. Phys. **93**, 57 (1984).